

MAXIMUM-LIKELIHOOD REPROJECTIONS FOR RELIABLE KOOPMAN-BASED PREDICTIONS AND BIFURCATION ANALYSIS OF PARAMETRIC DYNAMICAL SYSTEMS

PIETER VAN GOOR¹, ROBERT MAHONY², MANUEL SCHALLER³ AND KARL WORTHMANN⁴

ABSTRACT. Koopman-based methods leverage a nonlinear lifting to enable linear regression techniques. Consequently, data generation, learning and prediction is performed through the lens of this lifting, giving rise to a nonlinear manifold that is invariant under the Koopman operator. In data-driven approximation such as Extended Dynamic Mode Decomposition, this invariance is typically lost due to the presence of (finite-data) approximation errors. In this work, we show that reprojections are crucial for reliable predictions. We provide an approach via closest-point projections that ensure consistency with this nonlinear manifold, which is strongly related to a Riemannian metric and maximum likelihood estimates. While these results are already novel for autonomous systems, we present our approach for parametric systems, providing the basis for data-driven bifurcation analysis and control applications.

Keywords. Koopman operator, Extended Dynamic Mode Decomposition, parametric systems, consistency, maximum-likelihood, bifurcation.

1. INTRODUCTION

Lifting systems to higher dimensions is a key component of various data-driven methods. In Koopman-based approaches such as Extended Dynamic Mode Decomposition (EDMD), this lifting is performed by means of a dictionary of nonlinear functions [43], see also the recent overview of EDMD variants [6]. EDMD serves as a powerful data-driven tool for prediction [5, 9], control [2, 3, 16, 25, 36], model reduction [15] or spectral analysis [7, 8, 26, 27] revealing the central features (such as attractors) of the underlying nonlinear system.

In Koopman-based approaches, the dictionary used to lift the nonlinear finite-dimensional system to an infinite-dimensional linear one gives rise to a nonlinear manifold, the injective image of the original finite-dimensional state-space. This manifold is invariant under the action of the Koopman operator and formally one can study the dynamics of the original system as linear dynamics in the Koopman representation, relying on the invariance of the injective-manifold to preserve the state-representation. In particular, data generation, learning and prediction is performed purely through the lens of these functions. However, due to errors in data-driven and finite-dimensional approximations, this invariance is usually not preserved. Since the correspondence of dynamics is only correct on the injective manifold, this can quickly lead to significant instabilities and errors accumulating in predictions. Hence, in numerical implementations, a (re-)projection step is implicitly applied to maintain consistency, specifically by projecting back onto the manifold [23, 24], thereby mitigating deteriorating effects such as projection errors stemming from finitely many observable functions or estimation errors due to finitely many data points. After each prediction step of the linear model in the lifted space, the propagated observables are projected back onto the manifold before the surrogate model is used for the next prediction. When the coordinate functions are included in the dictionary,

¹Robotics and Mechatronics (RaM) Group, EEMCS Faculty, University of Twente, Netherlands
p.c.h.vangoor@utwente.nl.

²Systems Theory and Robotics Group, School of Engineering, The Australian National University, Australia
robert.mahony@anu.edu.au.

³Faculty of Mathematics, TU Chemnitz, Germany manuel.schaller@math.tu-chemnitz.de

⁴Optimization-based Control Group, Institute of Mathematics, Technische Universität Ilmenau, Germany
karl.worthmann@tu-ilmenau.de. K. Worthmann gratefully acknowledges funding by the Carl-Zeiss foundation within the project KI-MSO-O.

there is a canonical choice for this projection by provided by reading off the original state-coordinates from the the Koopman coordinate functions [39]. However, this may not be a particularly good choice of projection if the projective manifold is highly nonlinear. To the authors understanding, a structured analysis of reprojection methods is currently not available.

In this work, we provide a framework for a sophisticated choice of these reprojections onto the manifold by means of reprojections induced by a suitable metric. More precisely, we consider distances induced by weighting matrices that correspond to Riemannian metrics on the manifold. The widely-used coordinate projection can be interpreted as a closest-point reprojection with respect to a singular weighting matrix. Rather than this, we propose a weighting matrix that estimates the covariance of the underlying prediction error, allowing an interpretation as a maximum likelihood estimates.

The contribution of this paper is a geometric framework for reprojections for parametric systems addressing the following:

- (i) Analysis and interpretation of the geometric projection in view of maximum likelihood reprojections (Subsection 4.2); this was only sketched very briefly in the previous work [41].
- (ii) Extensive numerical case study in view of attractors and bifurcations in parametric systems (Subsection 4.3).
- (iii) Efficient implementation via adaptive reprojections in multi-step predictions (Subsection 5.1) and a Riemannian Newton method for the reprojection step (Subsection 5.2).

Outline. In Section 2 we provide the fundamentals of Koopman-based approximations. In Section 3, we recall reprojections onto the image of the dictionary to ensure consistency in data-driven approximations as outlined in [41]. The extension to the case of parameter-affine systems is provided in Section 4 which contains the main novel theoretical contributions of this work as well as a numerical study. Last, in Section 5, we provide an efficient implementation of the proposed method leveraging multistep predictions and a Riemannian Newton method.

2. THE KOOPMAN OPERATOR OF A DYNAMICAL SYSTEM AND ITS COMPRESSION

For an autonomous, locally-Lipschitz continuous vector field $f : \mathbb{R}^d \rightarrow \mathbb{R}^d$, the flow of f is denoted by $\text{Fl}_f^t : \mathbb{R}^d \rightarrow \mathbb{R}^d$ on its maximal interval of existence I , i.e., for every $x \in \mathbb{R}^d$, the flow map is defined by

$$\text{Fl}_f^0(x) = x, \quad \frac{d}{dt} \text{Fl}_f^t(x) = f(\text{Fl}_f^t(x)) \quad \forall t \in I.$$

Furthermore, let the compact and convex set $\mathbb{X} \subset \mathbb{R}^d$ be forward invariant with respect to the flow of f , i.e., the inclusion $\text{Fl}_f^t(x) \in \mathbb{X}$ holds for all $t \in I = [0, \infty)$. Then, the strongly-continuous Koopman semigroup of linear operators $(\mathcal{K}_f^t)_{t \geq 0}$ on $L^2(\mathbb{X}, \mathbb{R})$ is defined via the identity

$$(\mathcal{K}_f^t \varphi)(x) = \varphi(\text{Fl}_f^t(x)) \quad \forall x \in \mathbb{X}, \varphi \in L^2(\mathbb{X}, \mathbb{R}) \quad (2.1)$$

for all $t \in [0, \infty)$. We refer to elements $\varphi \in L^2(\mathbb{X}, \mathbb{R})$ as *observables*. The forward-invariance assumption on the set \mathbb{X} is imposed (and in the following tacitly used) to keep the presentation technically simpler, see, e.g., [45] for a detailed discussion. Otherwise, the Koopman operator \mathcal{K}_f^t maps observables defined on $f(\mathbb{X}) := \{y \in \mathbb{R}^d \mid \exists x \in \mathbb{X} : \text{Fl}_f^t(x) = y\}$, i.e., the image of the set \mathbb{X} under the flow, to observables defined on the set \mathbb{X} , see, e.g., [20] for details and ramifications with respect to multi-step predictions.

We briefly introduce EDMD as a method to compute a finite-dimensional approximation of the Koopman operator $\mathcal{K} = \mathcal{K}_f^t$ for an arbitrary, but fixed time step $t \in (0, \infty)$ and a given vector field f . To this end, one selects M linearly-independent observables $\psi_k \in L^2(\mathbb{X}, \mathbb{R})$, $k \in [1 : M]$. Then, we

refer to $\mathbb{V} := \text{span}\{\psi_i \mid i \in [1 : M]\}$ as the *dictionary* and define the vector-valued function

$$\Psi : \mathbb{X} \rightarrow \mathbb{R}^M, \quad x \mapsto (\psi_1(x) \dots \psi_M(x))^\top \quad (2.2)$$

such that for any $\varphi \in \mathbb{V}$, there is $a \in \mathbb{R}^M$ with $\varphi(x) = a^\top \Psi(x)$. The application of the Koopman operator \mathcal{K} to Ψ is to be understood componentwise, i.e., we set

$$\mathcal{K}\Psi = \begin{pmatrix} \mathcal{K}\psi_1 \\ \vdots \\ \mathcal{K}\psi_M \end{pmatrix} = \Psi(\text{Fl}_f^t(\cdot)) \in L^2(\mathbb{X}, \mathbb{R})^M \simeq L^2(\mathbb{X}, \mathbb{R}^M).$$

Then, we define the approximation $\hat{K} = \hat{K}_f^t$ of the Koopman operator $\mathcal{K} = \mathcal{K}_f^t$ over \mathbb{V} on the compact set \mathbb{X} as a best-fit solution in an L^2 -sense by means of the regression problem

$$\hat{K} = \arg \min_{K \in \mathbb{R}^{M \times M}} \int_{\mathbb{X}} \|\Psi(\text{Fl}_f^t(x)) - K\Psi(x)\|_2^2 dx. \quad (2.3)$$

The optimality conditions of (2.3) read: For all $\Phi \in \mathbb{V}^M$,

$$0 = \int_{\mathbb{X}} \langle \Psi(\text{Fl}_f^t(x)) - \hat{K}\Psi(x), \Phi(x) \rangle dx = \int_{\mathbb{X}} \langle \Psi(\text{Fl}_f^t(x)), \Phi(x) \rangle dx - \int_{\mathbb{X}} \langle \hat{K}\Psi(x), \Phi(x) \rangle dx$$

such that, using $\psi_i e_i \in \mathbb{V}^M$, $i \in [1 : M]$, as test functions, where $e_i \in \mathbb{R}^M$ is the i -th unit vector, the solution of Problem (2.3) can easily be calculated by

$$\hat{K} = \Psi_Y \Psi_X^{-1}, \quad (2.4)$$

where Ψ_X and Ψ_Y are given by $\Psi_X = \int_{\mathbb{X}} \Psi(x)\Psi(x)^\top dx$ and $\Psi_Y = \int_{\mathbb{X}} \Psi(\text{Fl}_f^t(x))\Psi(x)^\top dx$, respectively. Here, invertibility of the mass matrix Ψ_X follows from the linear independence of the observables, see [33, Lemma C.2]. The matrix \hat{K} is a representation of the compression of \mathcal{K} , i.e., $\hat{K} = P_{\mathbb{V}}\mathcal{K}|_{\mathbb{V}}$, where $P_{\mathbb{V}}$ is the L^2 -orthogonal projection onto \mathbb{V} . If the dictionary \mathbb{V} is Koopman-invariant, then $\hat{K} = \mathcal{K}|_{\mathbb{V}}$ holds. If this property is not satisfied, the projection $P_{\mathbb{V}}$ introduces a projection error, which was, to the best of our knowledge, first analyzed in [45] by means of a dictionary of finite elements, see also [34] for an extension to control systems. Using a kernel-based dictionary and the rich theory of reproducing kernel Hilbert spaces (RKHS), bounds on the projection error were provided in [32]. Recently, also pointwise error bounds in the context of regression in the RKHS norm (instead of the L^2 -norm) were given in [20] and also in [44] using a variant of EDMD with Bernstein polynomials.

Besides the above-mentioned projection error, in data-driven surrogates (corresponding to approximations of the integral by a sum over finitely many data points), an additional estimation error is introduced. We briefly comment on this topic, however we will keep the idealized situation (2.3) to illustrate the main contribution of this work.

Remark 2.1. *In fact, the regression problem (2.3) is the ideal formulation for the compression in the infinite-data limit. An empirical estimator of \hat{K} given $d \in \mathbb{N}$ i.i.d. data points x_1, \dots, x_d can be computed via*

$$\hat{K}_d = \arg \min_{K \in \mathbb{R}^{M \times M}} \sum_{j=1}^d \|\Psi(\text{Fl}_f^t(x_j)) - K\Psi(x_j)\|_2^2.$$

For $d \geq M$, $\hat{K}_{f,d} = (\Psi_X^d \Psi_Y^d) (\Psi_X^d \Psi_X^d)^\top)^{-1}$ is a closed-form solution using the $(M \times d)$ -data matrices Ψ_X^d and Ψ_Y^d with entries $\psi_k(x_j)$ and $\psi_k(\text{Fl}_f^t(x_j))$, $(k, j) \in [1 : M] \times [1 : d]$, respectively. The convergence $\hat{K}_d \rightarrow \hat{K}$ for $d \rightarrow \infty$ follows by the law of large numbers [17, 28]. For a quantitative convergence analysis and finite-data error bounds we refer to [19, 30, 33] for ergodic sampling,

also embedded in the general framework of operator learning, see [29] and [7, 18] for spectral approximation properties. For recent results on the estimation error in reproducing kernel Hilbert spaces, we refer to [32].

3. REPROJECTIONS TO ENSURE CONSISTENCY

Using the notation of Section 2, we define the immersed state manifold

$$\mathbb{M} := \text{im}(\Psi) = \{\Psi(x) \mid x \in \mathbb{X}\} \subset \mathbb{R}^M. \quad (3.1)$$

By definition, the set \mathbb{M} is *invariant* with respect to the Koopman operator \mathcal{K}_f^t , $t \in I = [0, \infty)$, in the sense that

$$(\mathcal{K}_f^t \Psi)(x) = \Psi(\text{Fl}_f^t(x)) \in \mathbb{M} \quad \forall x \in \mathbb{X} \quad (3.2)$$

holds, that is, the Koopman operator maps an \mathbb{M} -valued function to an \mathbb{M} -valued function. To fully preserve this property for the compression, see, e.g., [4] for an illustrative example and [41] for a more detailed discussion, Koopman invariance of the dictionary \mathbb{V} , i.e., if $\mathcal{K}\mathbb{V} \subseteq \mathbb{V}$, is needed since we then have $\hat{K} = P_{\mathbb{V}}\mathcal{K}|_{\mathbb{V}} = \mathcal{K}|_{\mathbb{V}}$. Clearly, finding such Koopman-invariant and still sufficiently expressive dictionary is of high interest as it can be inferred from [38] and the follow-up works, see, e.g., [13] and the references therein. Particularly interesting approaches are – among others, the development of a so-called consistency index in [14] and the use of neural networks in [12], which is also applicable for parameter-dependent dynamical systems. However, in general, one cannot expect $\hat{K}\Psi(x) \in \mathbb{M}$ for the approximated Koopman operator \hat{K} as depicted in Figure 1. This becomes even more prominent, if sensors serve as observables as it is typically the case in real-world systems.

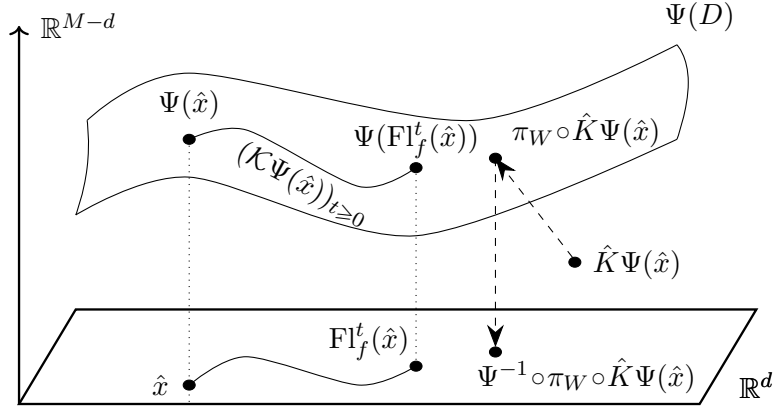


FIGURE 1. Geometric projection after applying the approximation \hat{K}_f .

This causes two issues in using \hat{K} (or data-driven approximations thereof) to model the flow of f :

- (1) The first is that it is unclear how to recover the state values underlying the propagated observables. Specifically, if $\hat{K}\Psi(x) \notin \mathbb{M}$, then by definition there is no value $x \in \mathbb{X} \subset \mathbb{R}^d$ satisfying $\Psi(x) = \hat{K}\Psi(x)$.
- (2) The second issue is that the learning process – based on the regression problem (2.3) – only uses measurements of the form $z = \Psi(x)$, i.e., only points contained in the set \mathbb{M} are taken into account. Hence, one cannot expect $\hat{K}z$ to be meaningful if $z \notin \mathbb{M}$, which may render a repeated application of \hat{K} questionable.

Both of these issues can be mitigated by *projecting* the dynamics $z^+ = \hat{K}z$, $z = \Psi(x)$, *back* to the set \mathbb{M} after each application of the Koopman operator, see, e.g., [23] and the follow-up work [24].

In this paper, we propose a framework for optimal choices of such reprojection maps including an extension to parameter-dependent systems. In particular, we discuss the following two choices: the widely used *coordinate projection* and our newly proposed *geometric projection*. Such a projection step is particularly crucial for future applications in Koopman-based (predictive) control using EDMDc [16] or a bilinear surrogate model [3, 42], where the construction of Koopman-invariant subspaces is a highly-nontrivial issue, see, e.g., [10].

In the conference paper [41], we formulated first steps towards reprojections for parameter-independent systems. Therein, we considered closest-point projections in weighted norms of the following type.

Definition 3.1. For a positive-definite matrix $W \in \mathbb{R}^{M \times M}$, the weighted reprojection $\pi_W : \mathbb{R}^M \rightarrow \mathbb{M}$ satisfies

$$\pi_W(z) \in \arg \min_{q \in \mathbb{M}} |q - z|_W^2 \quad (3.3)$$

with the weighted norm $|z|_W^2 := z^\top W z$. That is, for a point $z \in \mathbb{R}^M$, $\pi_W(z)$ provides the closest points in \mathbb{M} with respect to the norm induced by W .

Hence, after pursuing one or several steps along the data-driven model, we may reproject to the manifold \mathbb{M} by means of such a reprojection. In this work, we provide a thorough analysis of this idea addressing the following points:

- (1) Tailored application to parameter- or control-affine systems extending the results of [41] for autonomous systems.
- (2) Sophisticated data-driven choice of the weight matrix W by means of covariance matrices, allowing for a maximum likelihood interpretation of the projection π_W .
- (3) Efficient evaluation of (3.3) using Riemannian Newton methods leveraging the structure of the manifold \mathbb{M} .

This reprojection is optimal for recovering the state of the system in the sense that, if we take the model $\hat{K}\Psi(x)$ to be correct, then the most likely admissible state of the system is given by the reprojection $\pi_W(\hat{K}\Psi(x))$ upon a suitable choice of the weighting matrix W .

Proposition 3.2. Let $x \in \mathbb{X}$ and $z = \Psi(x) + \mu \subset \mathbb{R}^M$, where $\mu \sim N(0, \Sigma)$ for a positive definite covariance Σ . Then the maximum likelihood estimate $\hat{z} \in \mathbb{M}$ of $\Psi(x)$ given a measurement z satisfies

$$\hat{z} \in \pi_{\Sigma^{-1}}(z),$$

i.e., it is a weighted reprojection (3.3) with weighting matrix $W = \Sigma$.

Proof. Up to a constant offset, the negative log-likelihood of $\hat{z} = \Psi(x)$ given z is

$$l(\hat{z} = \Psi(x) | z) = \frac{1}{2} |z - \hat{z}|_{\Sigma^{-1}}^2.$$

An optimal solution for \hat{z} therefore satisfies $\hat{z} = \pi_{\Sigma^{-1}}(z)$. □

A widely-used and extremely simple form is the coordinate projection that was introduced, to the best of our knowledge, in [23].

Remark 3.3. Assume that the first d entries of the dictionary are the coordinate functions, i.e., $\Psi_i(x) = x_i$ for $i \in [1 : d]$. Then the weight function

$$W_c = \begin{pmatrix} I_d & 0 \\ 0 & 0 \end{pmatrix} \in \mathbb{R}^{M \times M}$$

induces a coordinate reprojection, that is,

$$\Psi(z_{[1:d]}) = \pi_{W_c}(z) \in \arg \min_{q \in \mathbb{M}} |q - z|_{W_c}^2,$$

where $z_{[1:d]} \in \mathbb{R}^d$ corresponds to the first d entries of $z \in \mathbb{R}^M$. For more details, i.e., a proof that W_c indeed induces a Riemannian metric on \mathbb{M} , we refer the reader to [41, Proposition 5.2].

4. REPROJECTIONS FOR PARAMETER-AFFINE SYSTEMS

We consider parameter-affine systems of the form

$$\dot{x} = f(x) + \sum_{i=1}^m p_i g_i(x), \quad (4.1)$$

where $f, g_1, \dots, g_m : \mathbb{X} \rightarrow \mathbb{R}^d$ are locally Lipschitz continuous vector fields and $p \in \mathbb{R}^m$, $m \in \mathbb{N}$, represents a constant parameter. An extension to parameter-varying problems (e.g. control systems) is straightforward such that in this work, we stick to the constant setting for ease of notation. In the following, for $p \in \mathbb{R}^m$ and $t \geq 0$, we denote by $\mathcal{K}_{f+\sum_{i=1}^m p_i g_i}^t$ the Koopman operator induced by (4.1), that is, for $x \in \mathbb{X}$ and $\varphi : \mathbb{X} \rightarrow \mathbb{R}$,

$$(\mathcal{K}_{f+\sum_{i=1}^m p_i g_i}^t \varphi)(x) = \varphi(\text{Fl}_{f+\sum_{i=1}^m p_i g_i}^t(x)),$$

again tacitly assuming that \mathbb{X} is invariant under $\text{Fl}_{f+\sum_{i=1}^m p_i g_i}^t$ for simplicity. Since one typically restricts parameter ranges to relatively small intervals, see, e.g., the examples below in Subsections 4.3.2 and 4.3.3, this is a reasonably mild assumption for dynamical systems.

4.1. The Koopman operator for parameter-affine systems. While the parameter-affine structure is directly inherited by the Koopman generator [31, 37, 42], see also [11] where this was leveraged for efficient learning on graphs, the Koopman operator is only approximately parameter-affine, as may be seen with a Taylor-series argument: For an observable $\varphi \in C^2(\mathbb{X}, \mathbb{R})$ and any $x \in \mathbb{X}$, one has

$$\begin{aligned} (\mathcal{K}_{f+\sum_{i=1}^m p_i g_i}^t \varphi)(x) &= \varphi(\text{Fl}_{f+\sum_{i=1}^m p_i g_i}^t(x)) \\ &= \varphi(x) + t \underbrace{\text{D}\varphi(x)(f + \sum_{i=1}^m p_i g_i)(x)}_{=\text{D}\varphi(x)f(x) + \sum_{i=1}^m p_i \text{D}\varphi(x)g_i(x)} + \mathcal{O}(t^2) \\ &= \left[\varphi(x) + t \text{D}\varphi(x)f(x) \right] + \sum_{i=1}^m p_i \left[t \text{D}\varphi(x)g_i(x) \pm \varphi(x) \right] + \mathcal{O}(t^2) \\ &= \varphi(\text{Fl}_f^t(x)) + \sum_{i=1}^m p_i \left[\varphi(\text{Fl}_{g_i}^t(x)) - \varphi(x) \right] + \mathcal{O}(t^2) \\ &= \mathcal{K}_f^t \varphi(\hat{x}) + \sum_{i=1}^m p_i (\mathcal{K}_{g_i}^t \varphi - \varphi)(x) + \mathcal{O}(t^2) \end{aligned}$$

Motivated by the above calculation and denoting by \otimes the usual Kronecker product we obtain the (infinite-dimensional) approximation for Ψ as defined in (2.2)

$$(\mathcal{K}_{f+\sum_{i=1}^m p_i g_i}^t \Psi)(x) = \bar{\mathcal{K}}^t(\bar{p} \otimes \Psi)(x) + \mathcal{O}(t^2), \quad (4.2)$$

with the augmented parameter vector $\bar{p} := \begin{pmatrix} 1 \\ p \end{pmatrix} \in \mathbb{R}^{m+1}$ and the column block operator

$$\bar{\mathcal{K}}^t := \begin{pmatrix} \mathcal{K}_f^t & \mathcal{K}_{g_1}^t - \mathcal{I} & \cdots & \mathcal{K}_{g_m}^t - \mathcal{I} \end{pmatrix}, \quad (4.3)$$

where \mathcal{K}_h^t , $h \in \{f, g_1, \dots, g_m\}$ is the Koopman operator corresponding to the flow Fl_h^t defined by (2.1).

This bilinear representation motivates the following (finite-dimensional) approximation

$$\hat{K} := \underset{K \in \mathbb{R}^{M \times M(m+1)}}{\text{argmin}} \int_{\mathbb{L} \otimes \mathbb{X}} \|\Psi(\text{Fl}_{f+\sum_{i=1}^m p_i g_i}^t(x)) - K(\bar{p} \otimes \Psi(x))\|_2^2 d(p \otimes x), \quad (4.4)$$

where $\mathbb{L} \subset \mathbb{R}^m$ is a compact set (with potentially only finitely-many elements) containing all possible parameters p . Solving the problem (4.4) yields an $M \times M(m+1)$ matrix that can be partitioned into

$$\widehat{K} = (\widehat{K}_0 \quad \widehat{K}_1 \quad \cdots \quad \widehat{K}_m) \quad (4.5)$$

with $\widehat{K}_i \in \mathbb{R}^{M \times M}$ for $i \in [0 : m]$, from which the individual approximations of the block-columns of $\bar{\mathcal{K}}^t$ in (4.3) can be defined. This leads to the approximation of the parametric Koopman operator

$$\left(\mathcal{K}_{f+\sum_{i=1}^m p_i g_i}^t \Psi \right) (x) = \Psi(\text{Fl}_{f+\sum_{i=1}^m p_i g_i}^t(x)) \approx \widehat{K}_0 \Psi(x) + \sum_{i=1}^m p_i \widehat{K}_i \Psi(x). \quad (4.6)$$

We stress that the structure of the right-hand side of (4.3) mainly serves as a motivation to formulate the regression problem (4.4) that may be leveraged in an error analysis.

As in the parameter-independent case (3.2), the parametric Koopman operator on the left-hand side of (4.6) preserves the set $\mathbb{M} = \Psi(\mathbb{X})$. However, as in the parameter-independent case, this does, in general, not hold for the approximation on the right-hand side of (4.6). Thus, the state of the approximating system must be reprojected to \mathbb{M} to recover a state of the original system in \mathbb{X} . Before presenting a suitable reprojection in Section 4.2, we briefly comment on data-driven surrogates of (4.4) via EDMD and provide a relation to existing parameter-affine approximations of the Koopman operator.

Remark 4.1.

- (i) *In the spirit of EDMD and analogously to Remark 2.1 we may perform a Monte-Carlo-like approximation of (4.4) by replacing the integral by a sum over data points, e.g., chosen i.i.d. with respect to the Lebesgue measure on $\mathbb{L} \otimes \mathbb{X}$.*
- (ii) *Following [32, Section 5], again using a Taylor-series argument, we have*

$$\begin{aligned} (\mathcal{K}_{g_i}^t \varphi - \varphi) (x) &= t \nabla \varphi \cdot (f + g_i - f)(x) + \mathcal{O}(t^2) \\ &= (\mathcal{K}_{f+g_i}^t \varphi - \varphi) (x) - (\mathcal{K}_f^t \varphi - \varphi) (x) + \mathcal{O}(t^2) \\ &= (\mathcal{K}_{f+g_i}^t \varphi) (x) - (\mathcal{K}_f^t \varphi) (x) + \mathcal{O}(t^2), \end{aligned}$$

which shows the equation

$$\mathcal{K}_f^t \varphi(\hat{x}) + \sum_{i=1}^m p_i (\mathcal{K}_{g_i}^t \varphi - \varphi) (\hat{x}) = \mathcal{K}_f^t \varphi(\hat{x}) + \sum_{i=1}^m p_i (\mathcal{K}_{f+g_i}^t \varphi - \mathcal{K}_f^t \varphi) (\hat{x}) + \mathcal{O}(t^2).$$

The presented line of reasoning allows us to replace the definition (4.3) by

$$\bar{\mathcal{K}}^t := (\mathcal{K}_f^t \quad \mathcal{K}_{g_1+f}^t - \mathcal{K}_f^t \quad \cdots \quad \mathcal{K}_{g_m+f}^t - \mathcal{K}_f^t), \quad (4.7)$$

which nicely links the presented parameter-affine approximation of the Koopman operator to existing ones [30, 31].

4.2. Maximum likelihood reprojections via covariance estimators. Consider the parameter-affine system (4.1) and let \mathbb{V} be a M -dimensional dictionary. Let $\Psi \in L^2(\mathbb{X}, \mathbb{R})^M$ denote the vector of observables spanning \mathbb{V} and \widehat{K} be the approximation of the Koopman operator defined in (4.4). Then, as discussed in Section 3, it is generally not guaranteed that the set $\mathbb{M} = \Psi(\mathbb{X})$ is preserved under the Koopman operator, compare (3.2). To measure the approximation error, the *residual operator* for a vector field f is defined on \mathbb{V} by

$$(\mathcal{R}_f^t \Psi)(x) := (\mathcal{K}_f^t \Psi)(x) - \widehat{K} \Psi(x),$$

where by \widehat{K}_f we denote the solution of (2.3).

Then, by virtue of the definition of \widehat{K} through the regression problem (2.3), the first and second moments of $\mathcal{R}_f^t \Psi$ satisfy

$$\begin{aligned}\mathbb{E}(\mathcal{R}_f^t \Psi) &= \int_{\mathbb{X}} \mathcal{R}_f^t \Psi(x) dx = \int_{\mathbb{X}} \Psi(\text{Fl}_f^t(x)) - \widehat{K} \Psi(x) dx = 0, \\ \text{Cov}(\mathcal{R}_f^t \Psi) &= \mathbb{E}((\mathcal{R}_f^t \Psi(x) - \mathbb{E}(\mathcal{R}_f^t \Psi))(\mathcal{R}_f^t \Psi(x) - \mathbb{E}(\mathcal{R}_f^t \Psi))^\top) \\ &= \int_{\mathbb{X}} \mathcal{R}_f^t \Psi(x) (\mathcal{R}_f^t \Psi(x))^\top dx \\ &= \int_{\mathbb{X}} (\Psi(\text{Fl}_f^t(x)) - \widehat{K} \Psi(x)) (\Psi(\text{Fl}_f^t(x)) - \widehat{K} \Psi(x))^\top dx.\end{aligned}$$

Here, we propose a model for the approximated Koopman dynamics as a linear system corrupted by a zero-mean Gaussian noise process, that is,

$$\Psi(\text{Fl}_f^t(x)) = \widehat{K}_f^t \Psi(x) + \mathcal{R}_f^t \Psi(x) \approx \widehat{K} \Psi(x) + \mu, \quad \mu \sim N(0, \text{Cov}(\mathcal{R}_f^t \Psi)).$$

While this is also an approximation, it captures the effects of the finite-dictionary Koopman fitting up to second-order. Moreover, it provides a stochastic approximation of the Koopman dynamics including a model of the error introduced by projection. In Proposition 4.2, we demonstrate how the covariance used to model the error can be computed from the same data used to construct \widehat{K} in the first place.

For parameter-dependent systems, we define the residual operator analogously, that is,

$$\mathcal{R}_{f+\sum_{i=1}^m p_i g_i}^t \Psi(x) := (\mathcal{K}_{f+\sum_{i=1}^m p_i g_i}^t \Psi)(x) - \left(\widehat{K}_0 + \sum_{i=1}^m p_i \widehat{K}_i \right) \Psi(x), \quad (4.8)$$

for all initial states $x \in \mathbb{X}$ and parameters $p \in \mathbb{L}$. Here, we recall that $\widehat{K}_i \in \mathbb{R}^{M \times M}$, $i \in [0 : m]$, are defined as the block columns of \widehat{K} , see (4.5), solving the augmented regression problem (4.4). For parameter-dependent systems (4.1), the covariance may depend on the parameter p in a non-trivial fashion. However, in the following, we will show that it can be approximated as a quadratic function of the parameters for short integration times. To this end, define the matrix-valued bilinear form $Q : \mathbb{R}^{m+1} \times \mathbb{R}^{m+1} \rightarrow \mathbb{R}^{M \times M}$ as the symmetric solution to the regression problem

$$\min_Q \int_{\mathbb{L}} \left\| \text{Cov}(\mathcal{R}_{f+\sum_{i=1}^m p_i g_i}^t \Psi) - Q(\bar{p}, \bar{p}) \right\|_F^2 dp, \quad (4.9)$$

where $\bar{p} = \begin{pmatrix} 1 \\ p \end{pmatrix} \in \mathbb{R}^{m+1}$ again denotes the augmented parameter vector. The solution Q may be determined analytically, that is, denoting by vec the column-wise vectorization of a matrix, Q solves (4.9) if

$$\text{vec}(Q(\bar{p}, \bar{p})) = Y X^\dagger (\bar{p} \otimes \bar{p}), \quad (4.10)$$

$$\text{where } Y := \int_{\mathbb{L}} \int_{\mathbb{X}} (\mathcal{R}_{f+\sum_{i=1}^m p_i g_i}^t \Psi(x) \bar{p}^\top) \otimes (\mathcal{R}_{f+\sum_{i=1}^m p_i g_i}^t \Psi(x) \bar{p}^\top) dx dp,$$

$$X := \int_{\mathbb{L}} \bar{p} \bar{p}^\top \otimes \bar{p} \bar{p}^\top dp.$$

Hereby we note that X may be computed analytically, where Y depends on the Koopman operator and thus has to be approximated by means of data in applications, see Remark 4.4.

The following result shows that the bilinear form Q yields a second-order approximation of the true covariance.

Proposition 4.2. *For any $p \in \mathbb{L}$, the covariance of the residual operator (4.8) satisfies*

$$\text{Cov} \left(\mathcal{R}_{f+\sum_{i=1}^m p_i g_i}^t \Psi \right) = Q(\bar{p}, \bar{p}) + \mathcal{O}(t^2), \quad (4.11)$$

where Q is defined as in (4.10).

Proof. For the expected value, we have that

$$\begin{aligned}\mathbb{E}(\mathcal{R}_{f+\sum_{i=1}^m p_i g_i}^t \Psi) &= \mathbb{E}(\mathcal{R}_f^t \Psi + \sum_{i=1}^m p_i \mathcal{R}_{g_i}^t \Psi) + \mathcal{O}(t^2) \\ &= \mathbb{E}(\mathcal{R}_f^t \Psi) + \sum_{i=1}^m p_i \mathbb{E}(\mathcal{R}_{g_i}^t \Psi) + \mathcal{O}(t^2) \\ &= \mathcal{O}(t^2)\end{aligned}$$

as $\mathbb{E}(\mathcal{R}_f^t \Psi) = \mathbb{E}(\mathcal{R}_{g_1}^t) = \dots = \mathbb{E}(\mathcal{R}_{g_m}^t) = \mathcal{O}(t^2)$. For convenience of notation, let $g_0 := f$, so that

$$f + \sum_{i=1}^m p_i g_i = \sum_{i=0}^m \bar{p}_i g_i.$$

Then, using the parameter-affine structure, the covariance satisfies

$$\begin{aligned}\text{Cov}(\mathcal{R}_{f+\sum_{i=1}^m p_i g_i}^t \Psi) &= \text{Cov}(\mathcal{R}_{\sum_{i=0}^m \bar{p}_i g_i}^t \Psi) \\ &= \text{Cov}\left(\sum_{i=0}^m \bar{p}_i \mathcal{R}_{g_i}^t \Psi\right) + \mathcal{O}(t^2) \\ &= \mathbb{E}\left(\left(\sum_{i=0}^m \bar{p}_i \mathcal{R}_{g_i}^t \Psi - \underbrace{\mathbb{E}\left(\sum_{i=0}^m \bar{p}_i \mathcal{R}_{g_i}^t \Psi\right)}_{=\mathcal{O}(t^2)}\right)\left(\sum_{i=0}^m \bar{p}_i \mathcal{R}_{g_i}^t \Psi - \underbrace{\mathbb{E}\left(\sum_{i=0}^m \bar{p}_i \mathcal{R}_{g_i}^t \Psi\right)}_{=\mathcal{O}(t^2)}\right)^\top\right) + \mathcal{O}(t^2) \\ &= \sum_{i,j=0}^m \bar{p}_i \bar{p}_j \mathbb{E}\left((\mathcal{R}_{g_i}^t \Psi)(\mathcal{R}_{g_j}^t \Psi)^\top\right) + \mathcal{O}(t^2).\end{aligned}\tag{4.12}$$

We now show that Q defined by (4.10) provides an approximation of the first term in (4.12) up to second order in t . To see this, we compute

$$\begin{aligned}Y &= \int_{\mathbb{L}} \int_{\mathbb{X}} (\mathcal{R}_{f+\sum_{i=1}^m p_i g_i}^t \Psi(x) \bar{p}^\top) \otimes (\mathcal{R}_{f+\sum_{i=1}^m p_i g_i}^t \Psi(x) \bar{p}^\top) dx dp \\ &= \int_{\mathbb{L}} \int_{\mathbb{X}} (\mathcal{R}_{\sum_{i=0}^m \bar{p}_i g_i}^t \Psi(x) \bar{p}^\top) \otimes (\mathcal{R}_{\sum_{i=0}^m \bar{p}_i g_i}^t \Psi(x) \bar{p}^\top) dx dp \\ &= \int_{\mathbb{L}} \int_{\mathbb{X}} ((\mathcal{R}_{g_0}^t \Psi(x) \dots \mathcal{R}_{g_m}^t \Psi(x)) \bar{p} \bar{p}^\top) \otimes ((\mathcal{R}_{g_0}^t \Psi(x) \dots \mathcal{R}_{g_m}^t \Psi(x)) \bar{p} \bar{p}^\top) dx dp + \mathcal{O}(t^2) \\ &= \int_{\mathbb{L}} \int_{\mathbb{X}} ((\mathcal{R}_{g_0}^t \Psi(x) \dots \mathcal{R}_{g_m}^t \Psi(x)) \otimes (\mathcal{R}_{g_0}^t \Psi(x) \dots \mathcal{R}_{g_m}^t \Psi(x))) (\bar{p} \bar{p}^\top \otimes \bar{p} \bar{p}^\top) dx dp + \mathcal{O}(t^2) \\ &= \int_{\mathbb{X}} ((\mathcal{R}_{g_0}^t \Psi(x) \dots \mathcal{R}_{g_m}^t \Psi(x)) \otimes (\mathcal{R}_{g_0}^t \Psi(x) \dots \mathcal{R}_{g_m}^t \Psi(x))) dx \int_{\mathbb{L}} (\bar{p} \bar{p}^\top \otimes \bar{p} \bar{p}^\top) dp + \mathcal{O}(t^2).\end{aligned}$$

Substituting this into the definition of Q , i.e., (4.10), we get

$$\begin{aligned}\text{vec}(Q(\bar{p}, \bar{p})) &= Y X^\dagger (\bar{p} \otimes \bar{p}) \\ &= \int_{\mathbb{X}} ((\mathcal{R}_{g_0}^t \Psi(x) \dots \mathcal{R}_{g_m}^t \Psi(x)) \otimes (\mathcal{R}_{g_0}^t \Psi(x) \dots \mathcal{R}_{g_m}^t \Psi(x))) dx (\bar{p} \otimes \bar{p}) + \mathcal{O}(t^2)\end{aligned}$$

$$\begin{aligned}
&= \int_{\mathbb{X}} ((\mathcal{R}_{g_0}^t \Psi(x) \cdots \mathcal{R}_{g_m}^t \Psi(x)) \bar{p}) \otimes ((\mathcal{R}_{g_0}^t \Psi(x) \cdots \mathcal{R}_{g_m}^t \Psi(x)) \bar{p}) \, dx + \mathcal{O}(t^2) \\
&= \int_{\mathbb{X}} (\mathcal{R}_{g_0}^t \Psi(x) p_0 + \cdots + \mathcal{R}_{g_m}^t \Psi(x) p_m) \otimes (\mathcal{R}_{g_0}^t \Psi(x) p_0 + \cdots + \mathcal{R}_{g_m}^t \Psi(x) p_m) \, dx + \mathcal{O}(t^2)
\end{aligned}$$

such that

$$\begin{aligned}
Q(\bar{p}, \bar{p}) &= \int_{\mathbb{X}} (\mathcal{R}_{g_0}^t \Psi(x) p_0 + \cdots + \mathcal{R}_{g_m}^t \Psi(x) p_m) (\mathcal{R}_{g_0}^t \Psi(x) p_0 + \cdots + \mathcal{R}_{g_m}^t \Psi(x) p_m)^\top \, dx + \mathcal{O}(t^2) \\
&= \sum_{i,j=0}^m \bar{p}_i \bar{p}_j \mathbb{E} \left((\mathcal{R}_{g_i}^t \Psi) (\mathcal{R}_{g_j}^t \Psi)^\top \right) + \mathcal{O}(t^2).
\end{aligned}$$

This completes the proof. \square

Combining Proposition 3.2 and Proposition 4.2, we directly obtain the following result for the parameter-dependent prediction model.

Corollary 4.3. *Let $x \in \mathbb{X}$ and $z = \Psi(x) \in \mathbb{M} \subset \mathbb{R}^M$. Let*

$$z^+ := \left(\hat{K}_0 + \sum_{i=1}^m p_i \hat{K}_i \right) z = \Psi(\text{Fl}_{f+\sum_{i=1}^m p_i g_i}^t(x)) + \mu, \quad \mu \sim N \left(0, \sum_{i,j=0}^m Q_{ij} p_i p_j \right).$$

Then, a maximum likelihood estimate $\hat{z}^+ \in \mathbb{M}$ of $\Psi(\text{Fl}_{f+\sum_{i=1}^m p_i g_i}^t(x))$ is given by

$$\hat{z}^+ \in \pi_{\Sigma^{-1}}(z^+) \quad \text{with} \quad \Sigma := \sum_{i,j=0}^m Q_{ij} p_i p_j.$$

We conclude this section commenting on data-driven approximations of the covariance surrogate Q .

Remark 4.4 (Data-driven approximation by EDMD). *To compute the matrix representation of Q serving as an approximation of the covariance matrix (4.11) similar to EDMD applied to the Koopman operator, we perform a Monte-Carlo approximation of the integrals appearing in (4.10) by a sum over finitely many data points.*

4.3. Numerical results. In this part, we present various numerical examples to illustrate the proposed parametric Koopman scheme and the corresponding reprojections. We discuss a scalar example in the subsequent Subsection 4.3.1, a two-dimensional Duffing oscillator in Subsection 4.3.2 and the three-dimensional Lorenz dynamics in Subsection 4.3.3. In all these examples, we discretize the ODE by means of a fourth-order Runge-Kutta method of fourth order with adaptive step-size control. For the evaluation, we distinguish three different cases of EDMD-based predictions:

- (i) Standard prediction without reprojection.
- (ii) Prediction with coordinate reprojection as described in Remark 3.3; applicable if the lifting map is injective.
- (iii) Maximum likelihood-based closest-point reprojection as proposed and outlined in Subsection 4.2.

In all numerical examples, if not stated otherwise, we approximate the Koopman operator using a polynomial dictionary up to order five with a sampling time step of $t = 0.1$.

4.3.1. Supercritical pitchfork bifurcation. First, we consider the scalar system

$$\frac{d}{dt}x(t) = px(t) - x(t)^3$$

with parameter $p \in \mathbb{R}$. This system corresponds to a supercritical pitchfork bifurcation, as with the parameter becoming positive, two stable equilibria arise. More precisely, we have the following two cases:

- (i) $p \leq 0$: The only equilibrium is the origin which is asymptotically stable.
- (ii) $p > 0$: The equilibria are given by $\{0, -\sqrt{p}, \sqrt{p}\}$, where the origin is unstable, and \sqrt{p} resp. $-\sqrt{p}$ are asymptotically stable for positive resp. negative initial values.

As a parameter and state domain, we choose $\mathbb{L} = \mathbb{X} = [-2, 2]$.

In Figure 2, we depict the scalar state (left) and the error over time (right). For $p = -1$, as depicted in the top row, we observe that the globally asymptotically stable nature of the origin renders all three Koopman-based predictions robust, that is, the error is relatively stable over the horizon. When transitioning to $p = 1$, however, we clearly see that a standard prediction fails after a short time period. In particular, while the formed equilibrium at $x = \sqrt{p} = 1$ is correctly identified using rejections, this is not the case for the standard prediction.

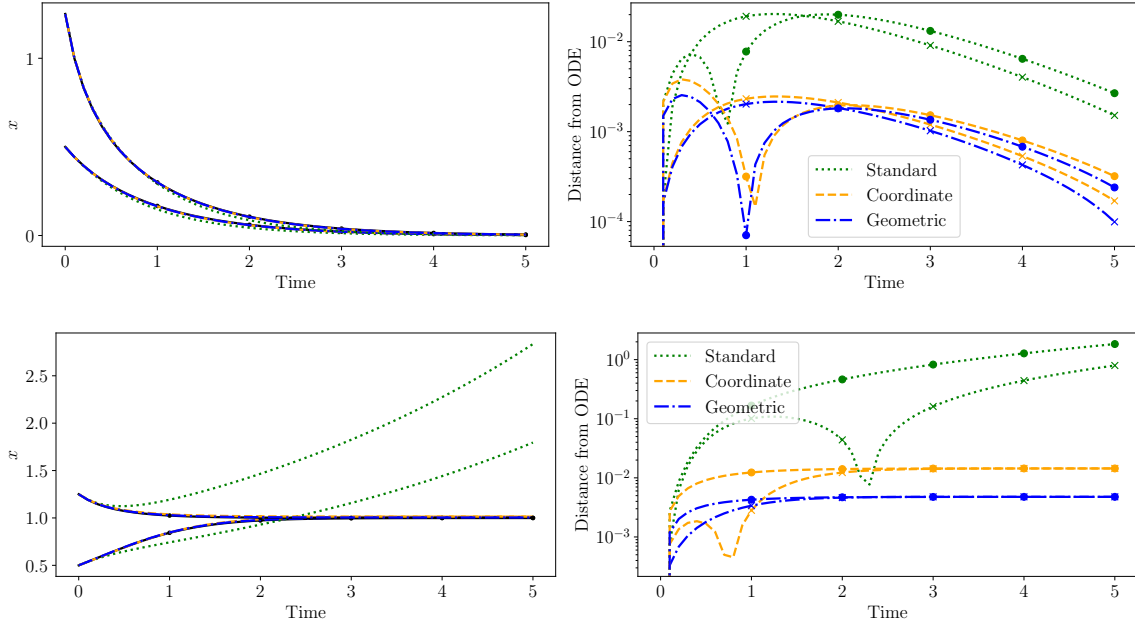


FIGURE 2. Pitchfork bifurcation for $p = -1$ (top) and $p = 1$ (bottom) for initial condition $x^0 = 0.5$ and $x^0 = 1.25$. Left: Trajectories over time. Right: Errors over time with $x^0 = 0.5$ marked by crosses and $x^0 = 1.25$ marked by bullets.

In Figure 3, we illustrate how the bifurcation at $p = 0$ is formed. The diagonal line illustrates the stability margin: If the dynamics is below this threshold, it is decreasing and if it is above this threshold, it is increasing. Consequently, the fixed points are then the intersection of the dynamics with the diagonal red line. We observe that, the bifurcation, the emerging fixed points and the corresponding stability behaviour is very well captured by both the coordinate and the maximum likelihood-based reprojction. The standard Koopman prediction does not capture the emerging fixed points and, as can be seen in the bottom left figure, also leads to a completely different stability behaviour in the interval $[-\sqrt{p}, \sqrt{p}]$.

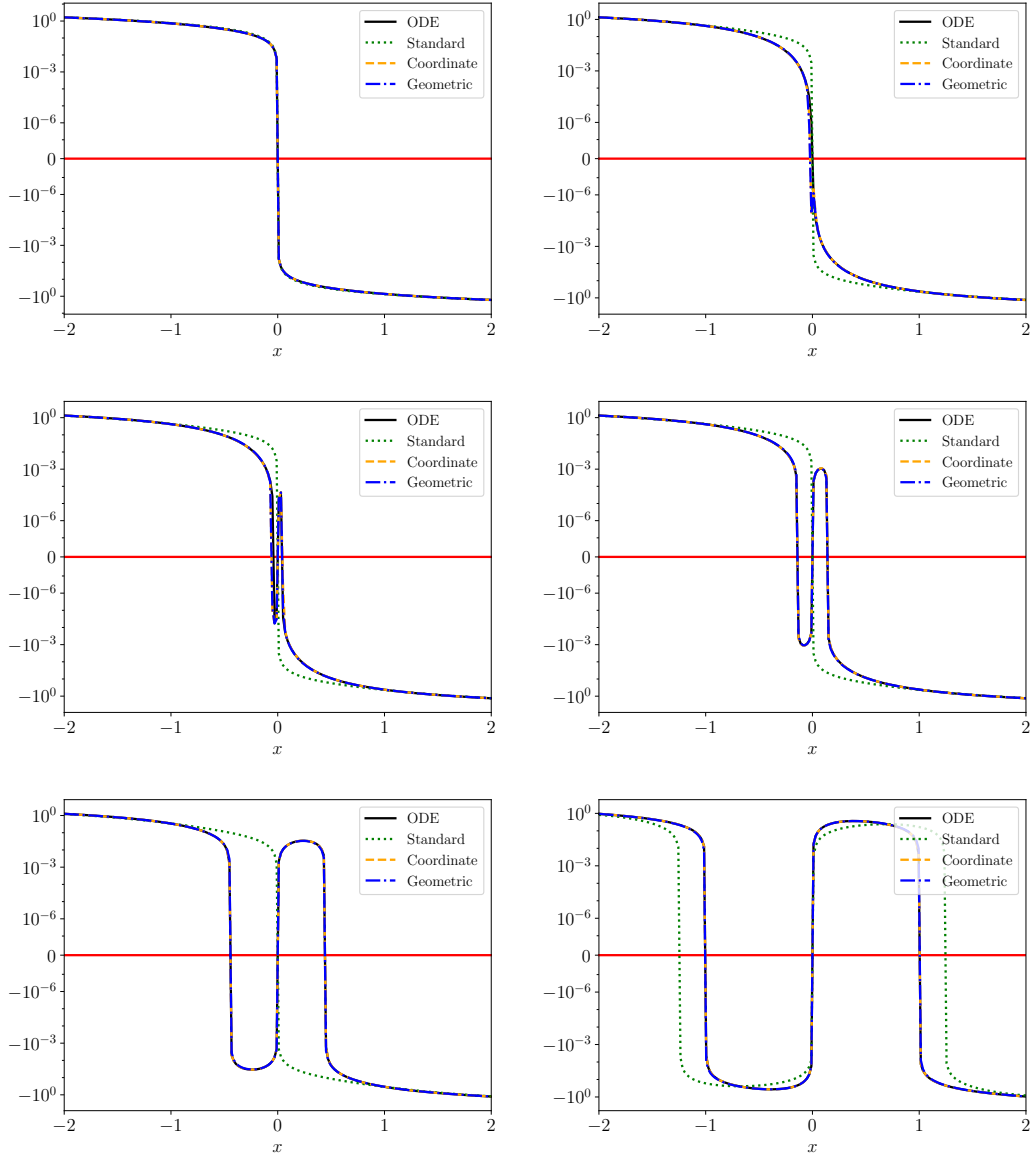


FIGURE 3. Pitchfork bifurcation: Illustration of bifurcation behaviour for $p \in \{-1, 0, 0.002, 0.02, 0.2, 1\}$ (row-wise).

4.3.2. *Duffing oscillator.* As a second example, we consider the two-dimensional Duffing oscillator

$$\frac{d}{dt} \begin{pmatrix} x_1(t) \\ x_2(t) \end{pmatrix} = \begin{pmatrix} x_2(t) \\ -\delta x_2(t) - \alpha x_1(t) - \beta x_1(t)^3 \end{pmatrix}$$

with fixed parameters $\delta = 0$ (no friction) and $\beta = 1$. As a varying parameter, we consider the stiffness $\alpha \in \mathbb{L} := [-2, 2]$.

In Figure 4, we again plot the performance of the three different Koopman-based predictions for four different stiffness parameters α . We observe that the standard prediction fails for all parameter choices, while the projection-based methods both perform well, even for stiffness $\alpha = -2.1$ outside

the parameter domain depicted in the top row. In particular, the errors remain relatively stable along the prediction horizon.

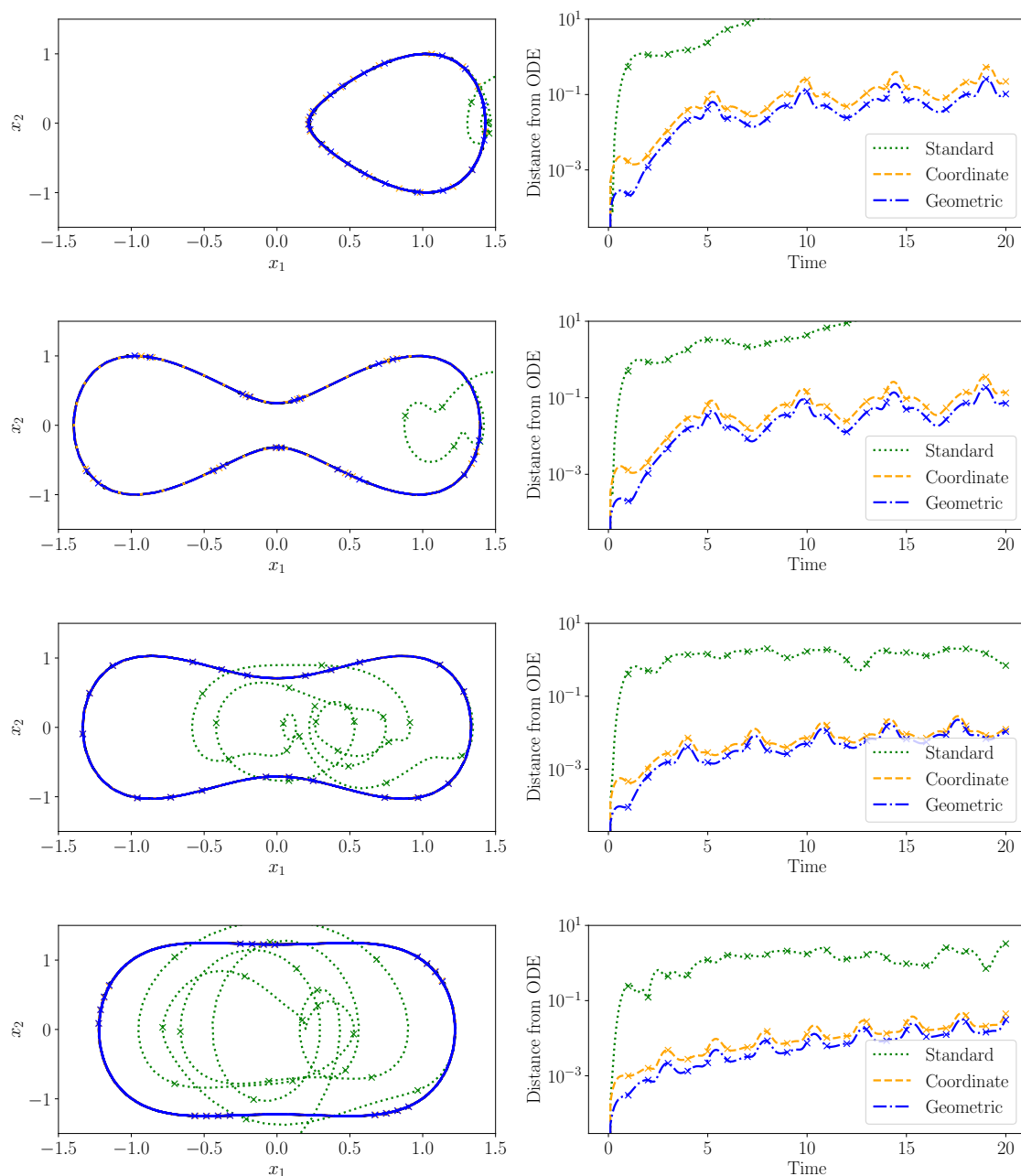


FIGURE 4. Different predictors for the parametric Duffing oscillator with $\alpha \in \{-2.1, -1.9, -1.5, -0.5\}$ (top to bottom)

4.3.3. *Lorenz attractor.* As a last example, we consider the three-dimensional Lorenz system given by

$$\dot{x}_1 = \sigma(x_2 - x_1), \quad \dot{x}_2 = x_1(\rho - x_3) - x_2, \quad \dot{x}_3 = x_1x_2 - \beta x_3$$

on the domain $\mathbb{X} = [-20, 20] \times [-20, 20] \times [10, 50]$. We fix $\sigma = 10$ and $\beta = 8/3$ and consider $\rho \in [10, 30]$ as a parameter. Note that the most common choice of the parameter giving rise to the well-known chaotic attractor is given by $\rho = 28$. As a time step, we choose $t = 0.01$ to capture the fast dynamics of the system and as a dictionary, we choose a monomial dictionary up to order three.

In Figure 5, we illustrate the formation of the attractor for different choices of the parameter ρ for the geometric reprojection. While the propagation using the standard Koopman model diverges already after a few time steps, we observe that the attractor is very well captured by the proposed geometric reprojection. The coordinate reprojection behaves very similarly to the geometric reprojection, which is why we only show the latter in Figure 5.

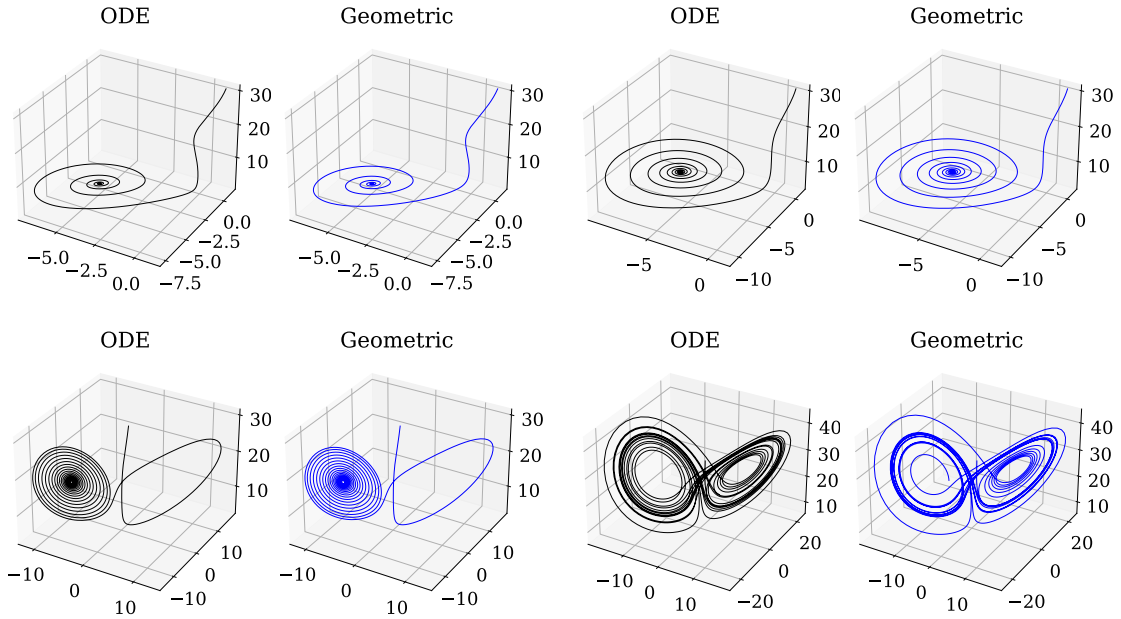


FIGURE 5. Formation of the Lorenz attractor by variations of the parameter $\rho \in \{8, 12, 18, 28\}$ (row-wise).

In Figure 6, we illustrate the results using a monomial dictionary without the first coordinate map. To obtain state predictions (and to define a coordinate projection), one may leverage injectivity of the lifting. More precisely, in the spirit of Remark 3.3, we may define a weighting matrix $W_c \in \mathbb{R}^{M \times M}$ by setting the diagonal entries corresponding to x_2, x_3 and x_1^3 to one, and the remainder to zero. We observe in Figure 6 that the geometric reprojection outperforms this coordinate reprojection. While long-term predictions depicted in Figure 5 worked well for both, the coordinate and the geometric reprojections in case of all coordinate functions contained in the dictionary $\mathbb{V} = \mathbb{V}_3$, in case of $\mathbb{V} = \mathbb{V}_3 \setminus x_1$, the larger error of the coordinate reprojection (depicted in Figure 6 leads to divergence already after a few time steps. Hence, when considering a dictionary that does not contain the coordinate functions, the geometric projection is the method of choice.

5. EFFICIENT IMPLEMENTATION

While the previous investigations showcased a favourable influence of the reprojection on the stability and accuracy of Koopman-based predictions, each evaluation requires the solution of a nonlinear minimization problem. In this section, we show how the numerical effort may be kept tractable by

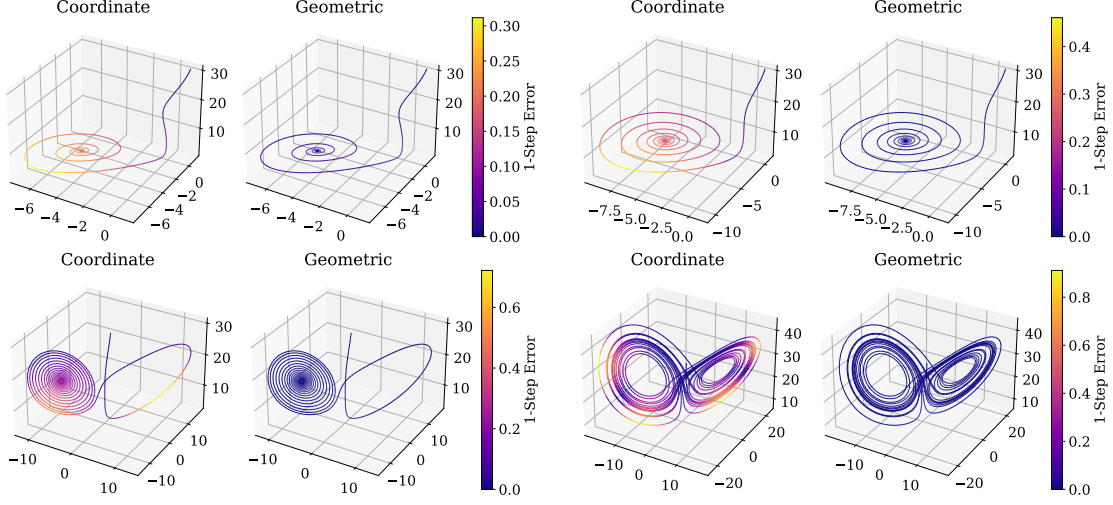


FIGURE 6. Formation of the Lorenz attractor by variations of the parameter $\rho \in \{8, 12, 18, 28\}$ (row-wise). Monomial dictionary without coordinate map of the first state, i.e., $\mathbb{V}_3 \setminus \{x_1\}$.

(i) reducing the number of projections required and (ii) providing an efficient numerical method to compute the projections.

To address (i), we propose an adaptive choice of the reprojection time in Subsection 5.1. In particular, we will follow the linear model for several time steps and then evaluate the projection only after a few time steps by means of an error estimator. Second, we formulate a Riemannian Newton method in Subsection 5.2. The nature of the problems to be solved being a series of optimization problems along a trajectory provides a very natural candidate for an initial guess enabling fast local convergence of the Newton method.

5.1. Multistep predictions. In this part, we employ the covariance model to provide a triggering condition for the reprojection step. This allows to conduct a reprojection only if needed; similarly to event-triggered mechanism for feedback linearization [40], or learning in general [35] conceptually following the sequential exploration-exploitation framework [22].

When considering data-driven multistep predictions, the lifted state $\hat{z}(k)$ follows

$$\hat{z}(k+1) = \left(\hat{K}_0 + \sum_{i=1}^m p_i \hat{K}_i \right) \hat{z}(k) \quad k = 0, 1, \dots$$

where $\hat{z}(0) = \Psi(x(0)) \in \mathbb{M}$ for an initial state $x(0)$. From the approximation (4.11), we have that

$$\left(\hat{K}_0 + \sum_{i=1}^m p_i \hat{K}_i \right) \Psi(x(k)) \approx \Psi(x(k+1)) + \mu,$$

where $\mu \sim N\left(0, \sum_{i,j=0}^m Q_{ij} p_i p_j\right)$.

Let $k \in \mathbb{N}$ be fixed and consider a prediction $\hat{z}(k) \in \mathbb{R}^M$ such that $\hat{z}(k) \approx \Psi(x(k)) + \eta_k$, where $\eta_k \sim N(0, \Sigma_k)$ for a given covariance Σ_k . Then,

$$\hat{z}(k+1) = \left(\hat{K}_0 + \sum_{i=1}^m p_i \hat{K}_i \right) \hat{z}(k)$$

$$\begin{aligned}
&= \left(\hat{K}_0 + \sum_{i=1}^m p_i \hat{K}_i \right) (\Psi(x(k)) + \eta_k) \\
&\approx \Psi(x(k+1)) + \mu_k + \left(\hat{K}_0 + \sum_{i=1}^m p_i \hat{K}_i \right) \eta_k.
\end{aligned}$$

It follows that

$$\begin{aligned}
\hat{z}(k+1) &\approx \Psi(x(k+1)) + \eta_{k+1} \\
\eta_{k+1} &\sim N \left(0, \sum_{i,j=0}^m Q_{ij} p_i p_j + \left(\hat{K}_0 + \sum_{i=1}^m p_i \hat{K}_i \right) \Sigma_k \left(\hat{K}_0 + \sum_{i=1}^m p_i \hat{K}_i \right)^\top \right). \quad (5.1)
\end{aligned}$$

In other words, the statistics of the error term η_{k+1} can be propagated using the parameters and the surrogate models. One can choose to perform reprojection only as needed, for example, when the covariance of η_k crosses a threshold. Note that to this end, we have to define a measure of the covariance, e.g., the trace of the matrix or diagonal entries corresponding of the covariance of particular variables.

In Figure 7, we depict the performance of the proposed multistep scheme for the scalar example of Subsection 4.3.1. To determine the prediction length, we only check the increase of the $(1, 1)$ -entry of the covariance matrix corresponding to the coordinate function.

In Figure 8, we illustrate the multistep predictions for the two-dimensional Duffing oscillator of Subsection 4.3.2. Here, we evaluate the trace of the covariance matrix and reproject if this uncertainty measure it increased by a pre-defined factor.

5.2. Efficient Reprojection via Riemannian Newton Method. In general, it is not straightforward to implement the proposed reprojection function (3.3). To use derivative-based methods for solving the corresponding *manifold-constrained nonlinear optimization problem*, we suppose that the image of Ψ defined in (3.1) has the structure of an embedded manifold.

Definition 5.1 (Embedded Submanifold [21, Chapter 4,5]). *An embedding of a manifold \mathbb{M} into \mathbb{R}^M is a smooth immersion $F : \mathbb{M} \rightarrow \mathbb{R}^M$ that is also a topological embedding. That is, F is smooth, the derivative $DF(x)$ has full rank for all $x \in \mathbb{M}$, and F is a homeomorphism onto its image $F(\mathbb{M}) \subseteq \mathbb{R}^M$. A manifold \mathbb{M} is called an embedded submanifold (of \mathbb{R}^M) if it is a subset $\mathbb{M} \subseteq \mathbb{R}^M$ and the inclusion map is an embedding.*

Assumption 5.2. *The map $\Psi : \mathbb{X} \rightarrow \mathbb{R}^M$ is an embedding; equivalently, $\mathbb{M} = \Psi(\mathbb{X}) \subset \mathbb{R}^M$ is an embedded submanifold.*

To apply optimization methods on the manifold \mathbb{M} , both a Riemannian metric on \mathbb{M} and a retraction from the tangent bundle $T\mathbb{M}$ are required. We recall the definitions as they are needed.

Definition 5.3 (Riemannian Metric [21, Chapter 13]). *For a manifold \mathbb{M} , a Riemannian metric on \mathbb{M} is a 2-tensor field g that is positive definite at each point. That is, for each $p \in \mathbb{M}$, the metric defines a positive definite bilinear map $g_p : T_p\mathbb{M} \times T_p\mathbb{M} \rightarrow \mathbb{R}$.*

The Riemannian metric may be simply inherited from the ambient Euclidean space; that is, for any $p \in \mathbb{M}$ and $\eta_1, \eta_2 \in T_p\mathbb{M}$, the Riemannian metric at p is defined by

$$g_p(\eta_1, \eta_2) := \langle \eta_1, \eta_2 \rangle, \quad (5.2)$$

where the right-hand side is the ordinary inner product in \mathbb{R}^M applied by the inclusion of $T_p\mathbb{M}$ as a subspace of \mathbb{R}^M .

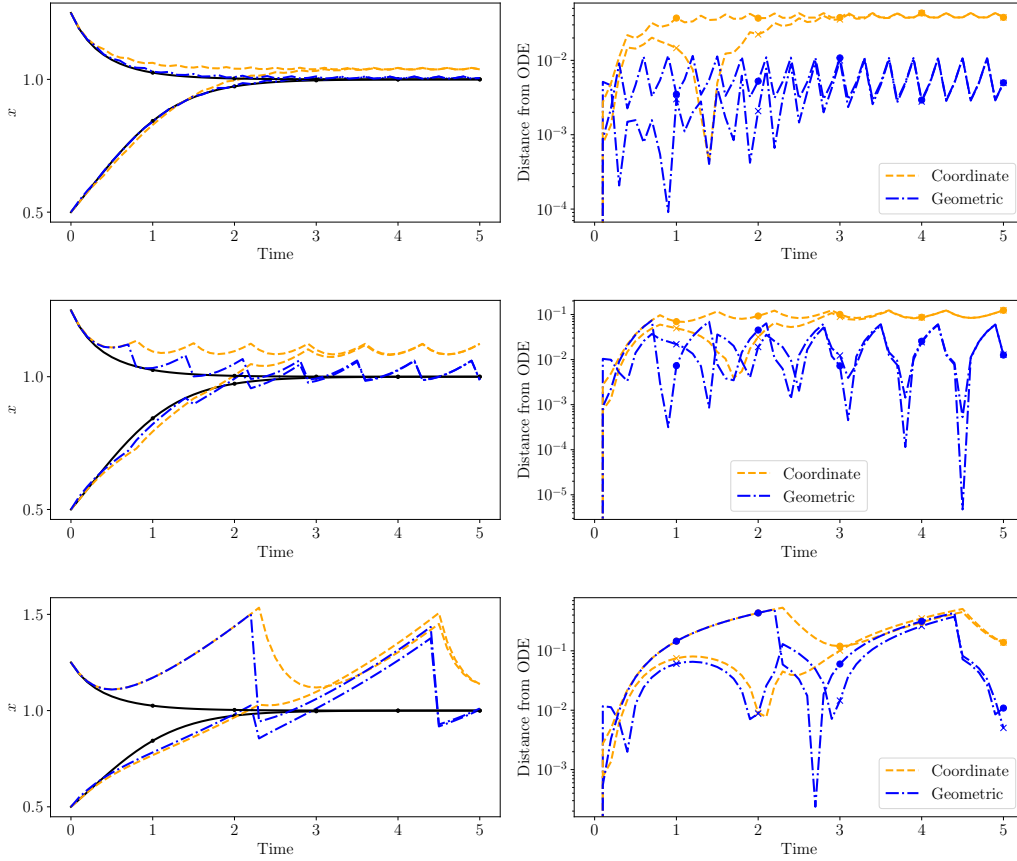


FIGURE 7. Pitchfork bifurcation with $p = 1$: Multistep predictions for a tolerance for the increase of the covariance by a factor in $\{10, 100, 1000\}$ leading to multi-stepping with $\{2, 6, 21\}$ steps (top to bottom). The error on the right is depicted for $x^0 = 0.5$ by crosses and for $x^0 = 1.25$ by bullets.

Definition 5.4 (Retraction [1, Definition 4.1.1]). A retraction on a manifold \mathbb{M} is a smooth map $R : T\mathbb{M} \rightarrow \mathbb{M}$ satisfying the following two properties, where $R_p : T_p\mathbb{M} \rightarrow \mathbb{M}$ is the restriction of R to $T_p\mathbb{M}$:

- (1) $R_p(0_p) = p$, where $0_p \in T_p\mathbb{M}$ is the zero vector in the tangent space at p .
- (2) Through the canonical identification $T_{0_p}T_p\mathbb{M} \simeq T_p\mathbb{M}$, the differential of R_p satisfies

$$DR_p(0_p) = \text{id}_{T_p\mathbb{M}},$$

where $\text{id}_{T_p\mathbb{M}} : T_p\mathbb{M} \rightarrow T_p\mathbb{M}$ denotes the identity map.

The definition of \mathbb{M} as the image of an embedding Ψ lends itself to defining a retraction.

Lemma 5.5. Consider the manifold $\mathbb{M} = \Psi(\mathbb{X}) \subset \mathbb{R}^M$. Define the map $R : T\mathbb{M} \rightarrow \mathbb{M}$ by

$$R_p(\eta) = \Psi(\Psi^{-1}(p) + D\Psi(\Psi^{-1}(p))^{-1}\eta),$$

for all $p \in \mathbb{M}$ and $\eta \in T_p\mathbb{M}$. Then R is a retraction.

Proof. Smoothness of R is immediate as it is a composition of smooth maps. Let $p \in \mathbb{M}$ be arbitrary and denote the zero element of the tangent space as $0_p \in T_p\mathbb{M}$. Then the retraction of the zero element

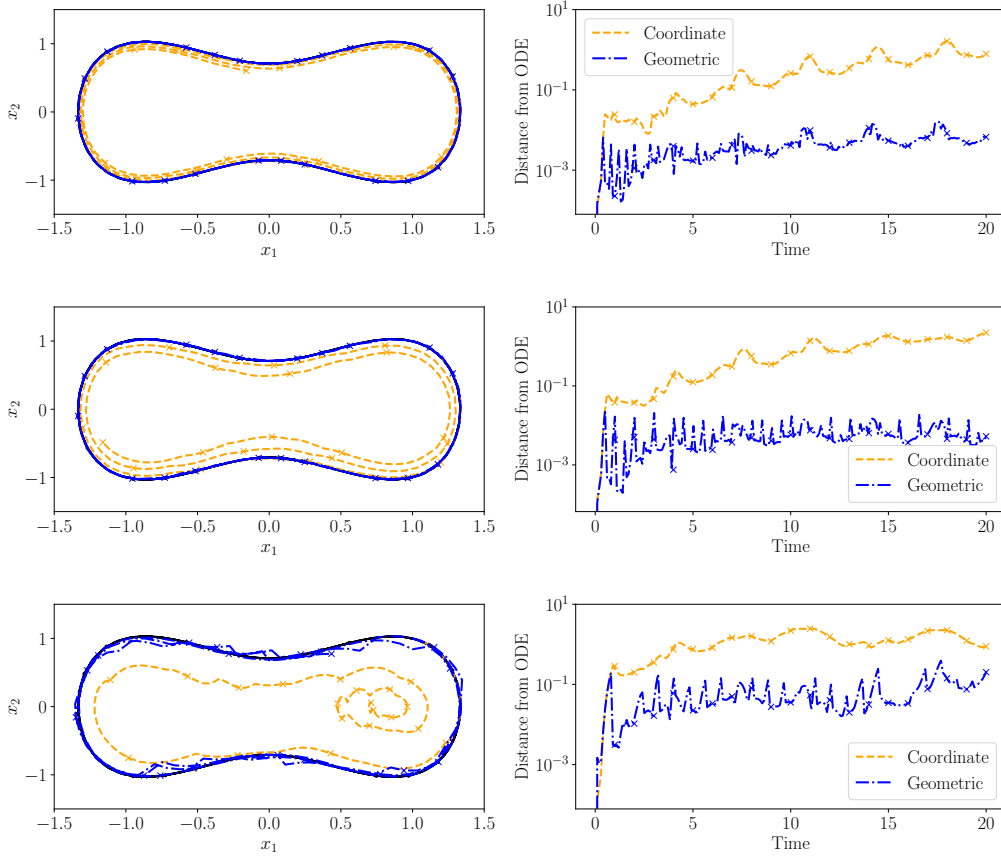


FIGURE 8. Duffing oscillator with $\alpha = -1.5$: Multistep predictions for a tolerance for the increase of the covariance by a factor in $\{10, 20, 30\}$ leading to multisteping with $\{3, 4, 7\}$ steps (top to bottom).

satisfies

$$R_p(0_p) = \Psi(\Psi^{-1}(p) + D\Psi(\Psi^{-1}(p))^{-1}0_p) = \Psi(\Psi^{-1}(p) + 0) = p.$$

Finally, for any $\eta \in T_{0_p}T_p\mathbb{M} \simeq T_p\mathbb{M}$,

$$\begin{aligned} DR_p(0_p)[\eta] &= \left. \frac{d}{dt} \right|_{t=0} R_p(0_p + t\eta) \\ &= \left. \frac{d}{dt} \right|_{t=0} \Psi(\Psi^{-1}(p) + D\Psi(\Psi^{-1}(p))^{-1}(0_p + t\eta)) \\ &= \left. \frac{d}{dt} \right|_{t=0} \Psi(\Psi^{-1}(p) + tD\Psi(\Psi^{-1}(p))^{-1}\eta) \\ &= D\Psi(\Psi^{-1}(p))D\Psi(\Psi^{-1}(p))^{-1}\eta \\ &= \eta. \end{aligned}$$

Thus $DR_p(0_p)$ is exactly the identity map on $T_p\mathbb{M}$ for all p . This shows that R is indeed a retraction. \square

Let $R : \mathbb{T}\mathbb{M} \rightarrow \mathbb{M}$ be the retraction defined in Lemma 5.5. Then we may apply a Riemannian Newton method [1, Algorithm 5] to find a local solution to the reprojection map π_W . Specifically, given a point $z \in \mathbb{R}^M$, define

$$l_z : \mathbb{M} \rightarrow \mathbb{R}, \quad l(p) := \frac{1}{2} |p - z|_W^2.$$

Then the Newton equation is

$$\text{Hess } l_z(p) \eta = -\text{grad } l_z(p). \quad (5.3)$$

The gradient and Hessian of l_z are easily computed to be

$$\text{grad } l_z(p) = W(p - z) \quad \text{Hess } l_z(p) = W,$$

using the embedded representation of $\mathbb{T}_p\mathbb{M}$. The Newton equation (5.3) thus appears trivial to solve by $\eta = (p - z)$. However, this neglects the fact that the Hessian and gradient of l_z are restricted to the tangent space of \mathbb{M} at p . This issue can be addressed by finding a minimal basis of the tangent space at p .

Let $x = \Psi^{-1}(p)$. Then the tangent space $\mathbb{T}_p\mathbb{M}$ is exactly the image of the differential $D\Psi(x) : \mathbb{R}^d \rightarrow \mathbb{R}^M$, and this map is injective. Therefore any $\eta \in \mathbb{T}_p\mathbb{M}$ may be written as $D\Psi(x)v$ for a unique $v \in \mathbb{R}^d$, and the standard basis vectors e_1, \dots, e_d of \mathbb{R}^d induce a basis $D\Psi(x)e_1, \dots, D\Psi(x)e_d \in \mathbb{R}^M$ for $\mathbb{T}_p\mathbb{M}$. In this basis, the gradient and Hessian may be written as

$$\text{grad } l_z(p) = D\Psi(x)^\top W(p - z) \quad \text{Hess } l_z(p) = D\Psi(x)^\top W D\Psi(x).$$

Let $v \in \mathbb{R}^d$ denote the unique vector in \mathbb{R}^d such that $\eta = D\Psi(x)v$. Then the Newton equation (5.3) simplifies to

$$D\Psi(x)^\top W D\Psi(x)v = -D\Psi(x)^\top W(p - z), \quad (5.4)$$

$$v = -(D\Psi(x)^\top W D\Psi(x))^\dagger D\Psi(x)^\top W(p - z). \quad (5.5)$$

The retraction of η can also then be simplified to

$$\begin{aligned} R_p(\eta) &= \Psi(\Psi^{-1}(p) + D\Psi(\Psi^{-1}(p))^{-1}\eta), \\ &= \Psi(\Psi^{-1}(p) + D\Psi(\Psi^{-1}(p))^{-1}D\Psi(x)v), \\ &= \Psi(\Psi^{-1}(p) + v). \end{aligned}$$

Finally, this leads to Algorithm 1 for obtaining $\pi_W(z)$.

Algorithm 1 features guaranteed local convergence. Specifically, if $x_* = \Psi^{-1}(p_*)$ is a critical point of $|p - z|_W^2$, then there is a neighbourhood \mathcal{U}_{x_*} of x_* such that, if $x_0 \in \mathcal{U}_{x_*}$ then the sequence x_k generated by the algorithm converges at least quadratically to x_* [1, Theorem 6.3.2].

The proposed algorithm requires an initial guess x_0 , which can be obtained through two simple approaches in practice. The first is to use a naive projection method such as coordinate projection. That is, if the coordinate functions are included in the dictionary \mathbb{V} , so that $\Psi(x) = (x, \bar{\Psi}(x))$, where $\bar{\Psi} : \mathbb{X} \rightarrow \mathbb{R}^{M-d}$, then the initial guess can be chosen as the first d coordinates of p , $x_0 := p_{1:d}$. Another possibility, which does not rely on a particular structure of the dictionary, is to use the previous value of $x^*(t_k)$ to initialise the guess for the new value $x_0(t_{k+1}) = x^*(t_k)$.

In Figure 9, we illustrate the superlinear convergence of the Riemannian Newton method for the projection. We observe that the tolerance of 10^{-8} is met already after a few time steps when using the solution of the previous time step as an initial guess. We conclude this section by means of a remark considering globalization.

Remark 5.6. *The Newton method proposed in Algorithm 1 can be extended to a trust region method such as [1, Algorithm 10] to provide global convergence under some mild assumptions.*

Algorithm 1 Riemannian Newton method for reprojection (3.3)**Require:** $W \in \mathbb{R}^{M \times M}$ positive semidefinite; $z \in \mathbb{R}^M$ the target point.**Goal:** Find $p \in \mathbb{M}$ to minimize $|p - z|_W^2$.**Input:** An initial guess $p_0 \in \mathbb{M}$.**Output:** An estimate \hat{p} of $\pi_W(z)$.

- 1: Set $x_0 = \Psi^{-1}(p_0) \in \mathbb{X}$.
- 2: **for** $k = 0, 1, 2, \dots, k_{\max}$ **do**
- 3: Solve the simplified Newton equation (5.4),

$$v_k = -(\mathrm{D}\Psi(x_k)^\top W \mathrm{D}\Psi(x_k))^\dagger \mathrm{D}\Psi(x_k)^\top W(p - z).$$

- 4: Set

$$\begin{aligned} x_{k+1} &= x_k + v_k, \\ \hat{p} &= \Psi(x_{k+1}). \end{aligned}$$

- 5: **if** $|v_k| \leq \text{threshold}$ **then**
- 6: **break**
- 7: **end if**
- 8: **end for**

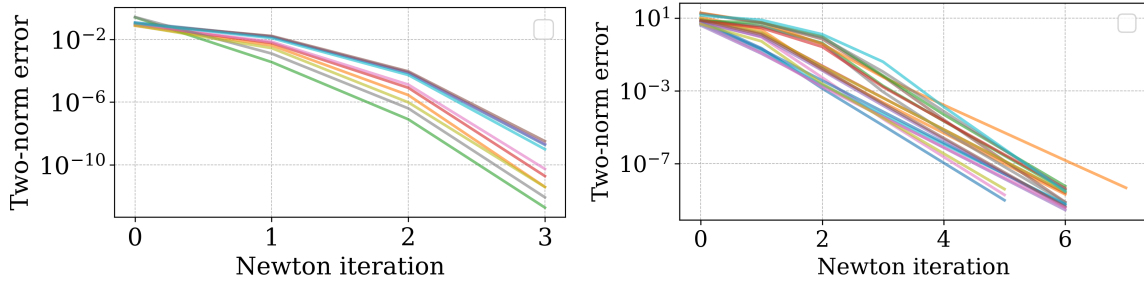


FIGURE 9. Error of Newton iteration for every 20th prediction step with time step $t = 0.1$ for the Duffing oscillator (left) and the Lorenz example (right).

6. CONCLUSION

In this paper, we proposed a reprojection method for Koopman-based predictions of nonlinear parameter-affine systems. Considering closest-point projections parametrized by weighting matrices mapping onto the consistent manifold of the compression, we have analyzed two particular choices corresponding to coordinate and maximum-likelihood projections and provided details for efficient implementation using an adaptive multistep scheme or a Riemannian Newton method. In various numerical examples, we have showcased the performance and increased robustness of Koopman-based predictions using these reprojections.

REFERENCES

- [1] Pierre-Antoine Absil, Robert Mahony, and Rodolphe Sepulchre. *Optimization algorithms on matrix manifolds*. Princeton University Press, 2009.
- [2] Petar Bevanda, Stefan Sosnowski, and Sandra Hirche. Koopman operator dynamical models: Learning, analysis and control. *Annual Reviews in Control*, 52:197–212, 2021.
- [3] Lea Bold, Lars Grüne, Manuel Schaller, and Karl Worthmann. Data-driven MPC with stability guarantees using extended dynamic mode decomposition. *IEEE Transactions on Automatic Control*, 70(1):534–541, 2025.

- [4] Steven L. Brunton, Bingni W. Brunton, Joshua L. Proctor, and J Nathan Kutz. Koopman invariant subspaces and finite linear representations of nonlinear dynamical systems for control. *PLoS one*, 11(2):e0150171, 2016.
- [5] Steven L. Brunton, Marko Budišić, Eurika Kaiser, and J. Nathan Kutz. Modern Koopman theory for dynamical systems. *SIAM Review*, 64(2):229–340, 2022.
- [6] Matthew J. Colbrook. The multiverse of dynamic mode decomposition algorithms. In *Numerical Analysis Meets Machine Learning*, volume 25 of *Handbook of Numerical Analysis*, pages 127–230. Elsevier, 2024.
- [7] Matthew J. Colbrook and Alex Townsend. Rigorous data-driven computation of spectral properties of Koopman operators for dynamical systems. *Communications on Pure and Applied Mathematics*, 77(1):221–283, 2024.
- [8] Gary Froyland, Georg A. Gottwald, and Andy Hammerlindl. A trajectory-free framework for analysing multiscale systems. *Physica D: Nonlinear Phenomena*, 328-329:34–43, 2016.
- [9] Dimitrios Giannakis and Suddhasattwa Das. Extraction and prediction of coherent patterns in incompressible flows through space–time Koopman analysis. *Physica D: Nonlinear Phenomena*, 402:132211, 2020.
- [10] Debdipta Goswami and Derek A Paley. Bilinearization, reachability, and optimal control of control-affine nonlinear systems: A Koopman spectral approach. *IEEE Transactions on Automatic Control*, 67(6):2715–2728, 2021.
- [11] Yang Guo, Manuel Schaller, Karl Worthmann, and Stefan Streif. Modularized data-driven approximation of the Koopman operator and generator. *Physica D: Nonlinear Phenomena*, 476:134651, 2025.
- [12] Yue Guo, Milan Korda, Ioannis G Kevrekidis, and Qianxiao Li. Learning parametric Koopman decompositions for prediction and control. *SIAM Journal on Applied Dynamical Systems*, 24(1):744–781, 2025.
- [13] Masih Haseli and Jorge Cortés. Learning Koopman eigenfunctions and invariant subspaces from data: Symmetric subspace decomposition. *IEEE Transactions on Automatic Control*, 67(7):3442–3457, 2021.
- [14] Masih Haseli and Jorge Cortés. Temporal forward–backward consistency, not residual error, measures the prediction accuracy of extended dynamic mode decomposition. *IEEE Control Systems Letters*, 7:649–654, 2022.
- [15] Stefan Klus, Feliks Nüske, Sebastian Peitz, Jan-Hendrik Niemann, Cecilia Clementi, and Christof Schütte. Data-driven approximation of the Koopman generator: Model reduction, system identification, and control. *Physica D: Nonlinear Phenomena*, 406:132416, 2020.
- [16] Milan Korda and Igor Mezić. Linear predictors for nonlinear dynamical systems: Koopman operator meets model predictive control. *Automatica*, 93:149–160, 2018.
- [17] Milan Korda and Igor Mezić. On convergence of extended dynamic mode decomposition to the Koopman operator. *Journal of Nonlinear Science*, 28(2):687–710, 2018.
- [18] Vladimir Kostic, Karim Lounici, Pietro Novelli, and Massimiliano Pontil. Sharp spectral rates for Koopman operator learning. *Advances in Neural Information Processing Systems*, 36, 2024.
- [19] Vladimir R Kostic, Karim Lounici, Prune Inzerilli, Pietro Novelli, and Massimiliano Pontil. Consistent long-term forecasting of ergodic dynamical systems. In *Proceedings of the 41st International Conference on Machine Learning*, volume 235, pages 25370–25395. PMLR, 2024.
- [20] Frederik Köhne, Friedrich M. Philipp, Manuel Schaller, Anton Schiela, and Karl Worthmann. L^∞ -error bounds for approximations of the Koopman operator by kernel extended dynamic mode decomposition. *SIAM Journal of Applied Dynamical Systems*, 24(1):501–529, 2025.
- [21] John M Lee. *Introduction to Smooth manifolds*. Springer, 2012.
- [22] Thomas Lew, Apoorva Sharma, James Harrison, Andrew Bylard, and Marco Pavone. Safe active dynamics learning and control: A sequential exploration–exploitation framework. *IEEE Transactions on Robotics*, 38(5):2888–2907, 2022.
- [23] Alexandre Mauroy and Jorge Goncalves. Linear identification of nonlinear systems: A lifting technique based on the Koopman operator. In *55th IEEE Conference on Decision and Control (CDC)*, pages 6500–6505, 2016.
- [24] Alexandre Mauroy and Jorge Goncalves. Koopman-based lifting techniques for nonlinear systems identification. *IEEE Transactions on Automatic Control*, 65(6):2550–2565, 2019.
- [25] Alexandre Mauroy, Igor Mezić, and Yoshihiko Susuki. *The Koopman operator in systems and control*. Springer Nature, Cham, Switzerland, 2020.
- [26] Igor Mezić. Analysis of fluid flows via spectral properties of the Koopman operator. *Annual Review of Fluid Mechanics*, 45:357–378, 2013.
- [27] Igor Mezić. Spectrum of the Koopman operator, spectral expansions in functional spaces, and state-space geometry. *Journal of Nonlinear Science*, 30(5):2091–2145, 2020.
- [28] Igor Mezić. On numerical approximations of the Koopman operator. *Mathematics*, 10(7):1180, 2022.
- [29] Mattes Mollenhauer, Stefan Klus, Christof Schütte, and Péter Koltai. Kernel autocovariance operators of stationary processes: Estimation and convergence. *Journal of Machine Learning Research*, 23(327):1–34, 2022.
- [30] Feliks Nüske, Sebastian Peitz, Friedrich Philipp, Manuel Schaller, and Karl Worthmann. Finite-data error bounds for Koopman-based prediction and control. *Journal of Nonlinear Science*, 33:14, 2023.
- [31] Sebastian Peitz, Samuel E Otto, and Clarence W Rowley. Data-driven model predictive control using interpolated Koopman generators. *SIAM Journal on Applied Dynamical Systems*, 19(3):2162–2193, 2020.

- [32] Friedrich Philipp, Manuel Schaller, Karl Worthmann, Sebastian Peitz, and Feliks Nüske. Error bounds for kernel-based approximations of the Koopman operator. *Applied and Computational Harmonic Analysis*, 71:101657, 2024.
- [33] Friedrich M. Philipp, Manuel Schaller, Septimus Boshoff, Sebastian Peitz, Feliks Nüske, and Karl Worthmann. Variance representations and convergence rates for data-driven approximations of Koopman operators. *Preprint arXiv:2402.02494*, 2024.
- [34] Manuel Schaller, Karl Worthmann, Friedrich Philipp, Sebastian Peitz, and Feliks Nüske. Towards reliable data-based optimal and predictive control using extended DMD. *IFAC-PapersOnLine*, 56(1):169–174, 2023.
- [35] Friedrich Solowjow and Sebastian Trimpe. Event-triggered learning. *Automatica*, 117:109009, 2020.
- [36] Robin Strässer, Manuel Schaller, Karl Worthmann, Julian Berberich, and Frank Allgöwer. Koopman-based feedback design with stability guarantees. *IEEE Transactions on Automatic Control*, 70(1):355–370, 2025.
- [37] Amit Surana. Koopman operator based observer synthesis for control-affine nonlinear systems. In *55th IEEE Conference on Decision and Control (CDC)*, pages 6492–6499, 2016.
- [38] Naoya Takeishi, Yoshinobu Kawahara, and Takehisa Yairi. Learning Koopman invariant subspaces for dynamic mode decomposition. *Advances in Neural Information Processing Systems*, 30, 2017.
- [39] Hiroaki Terao, Sho Shirasaka, and Hideyuki Suzuki. Extended dynamic mode decomposition with dictionary learning using neural ordinary differential equations. *Nonlinear theory appl. IEICE*, 12(4):626–638, 2021.
- [40] Jonas Umlauf and Sandra Hirche. Feedback linearization based on gaussian processes with event-triggered online learning. *IEEE Transactions on Automatic Control*, 65(10):4154–4169, 2019.
- [41] Pieter Van Goor, Robert Mahony, Manuel Schaller, and Karl Worthmann. Reprojection methods for Koopman-based modelling and prediction. In *62nd IEEE Conference on Decision and Control (CDC)*, pages 315–321, 2023.
- [42] Matthew O. Williams, Maziar S. Hemati, Scott T.M. Dawson, Ioannis G. Kevrekidis, and Clarence W. Rowley. Extending data-driven Koopman analysis to actuated systems. *IFAC-PapersOnLine*, 49(18):704–709, 2016.
- [43] Matthew O. Williams, Ioannis G Kevrekidis, and Clarence W Rowley. A data-driven approximation of the Koopman operator: Extending dynamic mode decomposition. *Journal of Nonlinear Science*, 25:1307–1346, 2015.
- [44] Rishikesh Yadav and Alexandre Mauroy. Approximation of the Koopman operator via Bernstein polynomials. *Communications in Nonlinear Science and Numerical Simulation*, page 108819, 2025.
- [45] Christophe Zhang and Enrique Zuazua. A quantitative analysis of Koopman operator methods for system identification and predictions. *Comptes Rendus. Mécanique*, 351(S1):1–31, 2023.